Available online at www.sciencedirect.com
SCIENCE DIRECT
Journal of Catalysis 238 (2006) 430–440
JOURNAL OF CATALYSIS
www.elsevier.com/locate/jcat

Effects of nanocrystalline CeO_2 supports on the properties and performance of Ni–Rh bimetallic catalyst for oxidative steam reforming of ethanol

Junichiro Kugai [a,1], Velu Subramani [a,2], Chunshan Song [a,*], Mark H. Engelhard [b], Ya-Huei Chin [b]

[a] *Clean Fuels and Catalysis Program, The Energy Institute, and Department of Energy and Geo-Environmental Engineering, The Pennsylvania State University, 209 Academic Projects Building, University Park, PA 16802, USA*

[b] *Environmental Molecular Sciences Laboratory, Pacific Northwest National Laboratory, Richland, WA 99352, USA*

Received 5 September 2005; revised 17 December 2005; accepted 3 January 2006

Available online 30 January 2006

Abstract

This study focuses on the effects of the CeO_2 support properties on the catalyst properties and performance of bimetallic Ni–Rh/CeO_2 catalysts containing 5 wt% Ni and 1 wt% Rh for the oxidative steam reforming (OSR) of ethanol for hydrogen production and fuel cell applications. Three CeO_2 supports with different crystal sizes and surface areas were examined. The surface areas of these supports increases in the order of CeO_2-I (74 m^2/g) < CeO_2-II (92 m^2/g) < CeO_2-III (154 m^2/g), but their crystallite sizes were about 10.2, 29.3, and 6.5 nm, respectively. The properties of Ni–Rh/CeO_2 catalysts were investigated by XRD, TPR, H_2 chemisorption, and in situ XPS techniques. The Rh metal dispersion increased while the Ni metal dispersion decreased with decreasing crystallite sizes of CeO_2. TPR studies revealed the existence of a Rh–CeO_2 metal–support interaction as well as Ni–Rh interaction in the Ni–Rh bimetallic catalyst supported on CeO_2-III with a crystallite size of about 6.5 nm. The in situ XPS studies corroborated the TPR results. The reduced Ni and Rh species were reversibly oxidized, suggesting the existence of Ni–Rh redox species rather than NiRh surface alloy in the present catalyst system. The Rh species became highly dispersed when the crystallite size of CeO_2 support was smaller. Comparing the catalytic performance in the OSR of ethanol with the properties of the catalysts demonstrated that both ethanol conversion and H_2 selectivity increased and the selectivity for undesirable byproducts decreased with increasing Rh metal dispersion. Best catalytic performance for OSR was achieved by supporting Ni–Rh bimetallic catalysts on the nanocrystalline CeO_2-III. The Ni–Rh/CeO_2-III catalyst exhibited stable activity and selectivity during on-stream operations at 450 °C and as well as at 600 °C.

Keywords: Ethanol; Reforming; Catalysis; CeO_2; Nano-size; Support; Crystallite size; Bimetallic; Catalysts; Ni–Rh; H_2 production; Bioethanol; Fuel cell application

1. Introduction

Reforming of alcohols and hydrocarbons has become an increasingly important and active area of catalysis research for hydrogen production and fuel cell applications [1–3]. Among various liquid hydrocarbon and alcoholic fuels, bioethanol (a mixture of water and ethanol produced from fermentation of biomass) has been considered an attractive alternative fuel. The research on H_2 production from renewable bioethanol is gaining increasing attention in recent years [4–15]. Most of the studies reported to date have used Al_2O_3-supported base metals or noble metals as catalysts for the reforming of ethanol and the reaction is operated at relatively higher reaction temperatures (around 700 °C) [6–11,13]. However, due to the thermodynamic equilibrium limitations, the high-temperature reforming produces a large amount of CO. This would require multi-stage water–gas shift (WGS) and preferential oxidation reactors downstream to produce H_2 suitable for proton-exchange membrane (PEM) fuel cells. To effectively integrate the ethanol reformer with PEM fuel cells, the reformer temperature should be as low as possible.

It has been shown recently that oxidative steam reforming (OSR) of ethanol (Eq. (1)), which combines steam reform-

* Corresponding author. Fax: +1 814 865 3248.
E-mail address: csong@psu.edu (C. Song).
[1] Present address: Nippon Shokubai Co. Ltd., 992-1 Aza Nishioki Okihama, Aboshi-ku Himeji Hyogo 671-1292, Japan.
[2] Present address: Center for Energy Technology, Research Triangle Institute, Research Triangle Park, NC 27709, USA.

0021-9517/$ – see front matter
doi:10.1016/j.jcat.2006.01.001

ing (Eq. (2)) and partial oxidation (Eq. (3)), is more effective and energy efficient compared with the conventional steam-reforming reaction [4,11–13]:

$$CH_3CH_2OH(l) + (3-2\delta)H_2O(l) + \delta O_2(g) \rightarrow (6-2\delta)H_2(g) + 2CO_2(g), \quad (1)$$

if $\delta = 0.6$, $\Delta H^0_{298} = +4.4\ \mathrm{kJ\,mol^{-1}}$;

$$CH_3CH_2OH(l) + 3H_2O(l) \rightarrow 6H_2(g) + 2CO_2(g), \quad (2)$$

$\Delta H^0_{298} = +347.4\ \mathrm{kJ\,mol^{-1}}$;

$$CH_3CH_2OH(l) + 1.5O_2(g) \rightarrow 3H_2(g) + 2CO_2(g), \quad (3)$$

$\Delta H^0_{298} = -554.0\ \mathrm{kJ\,mol^{-1}}$.

Recently we reported novel Ni–Rh bimetallic catalysts on a CeO_2 support for low-temperature oxidative steam reforming of ethanol to produce H_2 with high selectivity and low CO in the outlet [15,16]. The Ni and Rh loadings, as well as the reaction operating conditions, were tailored to achieve higher ethanol conversion and better H_2 selectivity at relatively lower operating temperatures (around 400 °C). However, the influential factors associated with the CeO_2 support that affect the catalytic activity and selectivity for ethanol reforming over Ni–Rh/CeO_2 catalysts have not yet been studied.

Consequently, the objective of the present study was to explore how the CeO_2 support properties affect the catalyst properties and performance of Ni–Rh/CeO_2 bimetallic catalysts in the OSR of ethanol. Three different CeO_2 supports were selected and examined, because some important catalyst properties may depend on the specific surface area and crystallite sizes of support. The Ni–Rh catalysts were compared in the OSR of ethanol under similar reaction conditions and the results correlated with their properties, as characterized by temperature-programmed reduction (TPR), H_2 chemisorption, X-ray diffraction (XRD), and in situ X-ray photoelectron spectroscopy (XPS) techniques.

2. Experimental

2.1. Preparation of catalysts

Three different CeO_2 supports were used. CeO_2-I was prepared by calcination of cerium nitrate at 600 °C; CeO_2-II was obtained from Sigma–Aldrich, and CeO_2-III was obtained from Rhodia Chemicals. Ni–Rh/CeO_2 catalysts were prepared by incipient wetness coimpregnation [15,16]. Aqueous solutions of Ni(II) nitrate and Rh(III) chloride salts were used as precursors of Ni and Rh metals for nominal loadings of 5 and 1 wt%, respectively. The impregnated samples were dried at 100 °C for 6–8 h and then calcined at 450 °C for 3 h in a temperature-programmed muffle furnace using a ramp rate of $2\ ^\circ\mathrm{C\,min^{-1}}$. Note that other Rh precursors exist besides the $RhCl_3$ used in this study, and the precursor type may affect the properties of the resulting catalyst.

2.2. Catalyst characterization

The BET surface area and pore size distribution of the catalysts were measured by N_2 adsorption at liquid N_2 temperature using a Micromeritics ASAP 2010 instrument. XRD patterns of calcined samples were recorded on a Scintag 2 powder diffractometer using Cu-K_α radiation at a scan rate of $4^\circ\ \mathrm{min^{-1}}$ in the 2θ range of 5°–70°. For the analysis of CeO_2 crystallite size, the XRD data were collected at a low scan rate of $0.5^\circ\ \mathrm{min^{-1}}$ in the 2θ range of 25°–30° covering the CeO_2(111) diffraction peak at 28.6°. The crystallite sizes were calculated using Scherrer's equation, $t = (0.9\lambda)/(\beta\cos\theta)$, where t is the crystallite size, λ is the wavelength of the radiation, β is the full-width at half maximum (FWHM) of the CeO_2(111) peak in radian, and θ is the Bragg diffraction angle.

TPR was conducted on a Micromeritics AutoChem 2910 TPD/TPR instrument as described previously [15,16]. The Ni and Rh metal surface areas and their dispersions were determined by H_2 pulse chemisorption experiments performed on the same Micromeritics instrument used for the TPR study. As a general procedure, about 100 mg of Ni–Rh/CeO_2 sample (35–60 mesh) was loaded in a quartz reactor and reduced at 160 °C for 2 h in a pure H_2 stream of 50 $\mathrm{cc\,min^{-1}}$ at a ramp rate of $5\ ^\circ\mathrm{C\,min^{-1}}$. The sample was then flushed with He gas and cooled to ambient temperature (50 °C). The reduced sample was then saturated with H_2 by pulsing a 25% H_2/Ar mixture. The amount of H_2 chemisorbed was monitored by a thermal conductivity detector and a computer data acquisition system provided in the instrument.

Based on TPR, a "sequential H_2 pulse chemisorption" method was designed and used to separately determine the metal surface area and particle sizes of Rh and Ni in the bimetallic catalysts. The H_2 consumption for Rh was determined in the first cycle by reducing the catalyst at 160 °C for 2 h, where mainly Rh^{3+} was reduced and dispersed on the CeO_2 support. The same sample was subsequently reduced at 450 °C for 2 h, where both Rh^{3+} and Ni^{2+} species were reduced. The H_2 uptake in the second cycle was the total H_2 uptake, corresponding to both Rh and Ni metals. The H_2 uptake for Ni metal was determined from the data obtained from the second cycle by substracting the value for Rh metal in the first cycle. The H_2 consumption due to surface-reduced CeO_2 was considered negligible, at least up to 160 °C in the first cycle for the chemisorption on Rh. The metal surface area, dispersions, and particle sizes were calculated from the H_2 uptake in the first and second cycles using a stoichiometric factor of 2 (1 mol of H_2 for 2 mol of metal atoms) for both Rh and Ni.

XPS measurements of both unreduced and reduced catalysts were performed by a pseudo-in situ method at the Pacific Northwest National Laboratory. About 100 mg of the catalyst was loaded in a quartz reactor and reduced under a 5% H_2/Ar mixture ($50\ \mathrm{cc\,min^{-1}}$) at a ramp rate of $4\ ^\circ\mathrm{C\,min^{-1}}$ up to 433 °C and kept at this temperature for 1 h before cooling to room temperature. The reactor was sealed and transferred into a glove box with O_2 concentration maintained below 0.5 ppm. In the glove box, the reduced catalysts were retrieved and mounted for XPS analysis. The XPS measurements were performed using a Physical Electronics Quantum 2000 Scanning ESCA microprobe with an attached high-purity nitrogen-purged glove bag. The system used a focused monochromatic Al-K_α X-ray (1486.7 eV) source for excitation and a spherical section an-

alyzer [17]. The X-ray beam used for this data was a 105-W, 100-μm X-ray beam spot rastered over a 1.4 × 0.2 mm rectangle on the sample. Data were collected using a pass energy of 46.95 eV. Although the binding energy (BE) scale was calibrated using the Cu $2p_{3/2}$ feature at 932.62 ± 0.05 eV and Au 4f at 83.96 ± 0.05 eV for known standards, the catalysts experienced variable degrees of charging depending on the extent of oxidation. Electrons of 1 eV, 20 μA, and low-energy Ar^+ ions were used to minimize this charging, and BE positions were referenced using 917.0 eV for the Ce $3d_{3/2}$ $4f^0$ feature.

2.3. Catalytic studies

The catalytic performance in the OSR of ethanol was evaluated at 300–600 °C at atmospheric pressure using a stainless steel fixed-bed flow reactor as described elsewhere [15]. About 100 mg of catalyst sieved to 35–60 mesh was packed in the reactor. A premixed ethanol–water mixture with a water/ethanol molar ratio of 4/1 was fed into the reactor through a vaporizer, where it was heated, vaporized, and mixed with Ar carrier gas and air (O_2/EtOH ratio = 0.4). The flow rate of Ar carrier gas was adjusted to maintain the total gas/EtOH at 10/1. Before the catalytic reaction, the catalysts were reduced in situ under H_2 flow (10% H_2 in Ar) at 435 °C for 2 h. The effluent gas of the reaction was analyzed using two on-line gas chromatographs (SRI Model 8610C), one equipped with a thermal conductivity detector for the gas analysis using a Molecular Sieve 5A and silica gel-packed columns, and the other with a flame ionization detector for the analysis of liquid products using a 7% Carbowax/Carbograph packed column.

Thermodynamic analysis for the OSR of ethanol was performed using HSC Chemistry V. 3.02 (Outokumpu Software). The equilibrium composition was calculated under the same conditions (initial feed-gas composition, temperature, ambient pressure) as the actual reaction conditions.

3. Results

3.1. Physicochemical properties

3.1.1. Structural and textural properties

Table 1 gives the BET surface area and porosity values of different CeO_2 supports and catalysts. The surface areas of the samples before Ni and Rh impregnation increased in the following order: CeO_2-I < CeO_2-II < CeO_2-III. Note that Gorte et al. [18,19] used CeO_2 support derived from thermal decomposition of $Ce(NO_3)_3{\cdot}6H_2O$ salt at 600 °C with a specific surface area of about 37 m^2/g as determined by 2-propanol adsorption. The three different CeO_2 samples of the present study were used for supporting 5 wt% Ni and 1 wt% Rh. On Ni and Rh loading, the BET surface areas of CeO_2-I and CeO_2-III decreased by up to 12 and 17%, respectively, and that of CeO_2-II decreased by about 27%. A significant loss in pore volume was also observed in the latter sample.

The XRD patterns of the CeO_2-supported Ni–Rh bimetallic catalysts are shown in Fig. 1. The catalysts exhibit phase corresponding to mainly CeO_2. The CeO_2 crystallite size calculated from line-broadening experiments decreased in the following order: Ni(5)Rh(1)/CeO_2-II (29.3 nm) > Ni(5)Rh(1)/CeO_2-I (10.2 nm) > Ni(5)Rh(1)/CeO_2-III (6.5 nm). These values are in accordance with the relative intensity of the XRD peaks. As can be seen, Ni(5)Rh(1)/CeO_2-II exhibits sharp peaks with high intensity, whereas Ni(5)Rh(1)/CeO_2-III shows broad and less intense peaks. A separate Rh_2O_3 phase was not found on XRD; however, the appearance of a small hump at around 43° 2θ in the Ni(5)Rh(1)/CeO_2-I and Ni(5)Rh(1)/CeO_2-II samples indicates the presence of a NiO phase. Because the XRD line of the NiO phase was very weak and close to the background noise, it was not possible to determine its crystallite size. The observed results seem to suggest that nanoparticles of NiO and Rh_2O_3 (particle sizes <5 nm, undetectable by XRD) are present on the CeO_2 support [20].

Table 2 summarizes H_2 chemisorption data on the various CeO_2-supported Ni–Rh bimetallic catalysts. The H_2 up-

Table 1
Physicochemical properties of CeO_2 supported Ni–Rh bimetallic catalysts

Catalyst[a]	S_{BET}[b] ($m^2\ g^{-1}$)	Pore volume[b] ($ml\ g^{-1}$)	Average pore diameter[b] (nm)	CeO_2 crystallite size[c] (t) (nm)
Ni(5)Rh(1)/CeO_2-I	65	0.174	10.7	10.2
CeO_2-I	74	0.200	10.7	–
Ni(5)Rh(1)/CeO_2-II	67	0.104	6.2	29.3
CeO_2-II	92	0.413	17.9	–
Ni(5)Rh(1)/CeO_2-III	128	0.119	3.7	6.5
CeO_2-III	154	0.131	3.4	–

[a] CeO_2-I was obtained from thermal decomposition of $Ce(NO_3)_3$. CeO_2-II and CeO_2-III were obtained from Sigma–Aldrich and Rhodia Chemical Company, respectively.
[b] Determined from N_2 adsorption–desorption measurements.
[c] Calculated from CeO_2(111) reflection employing Scherrer equation.

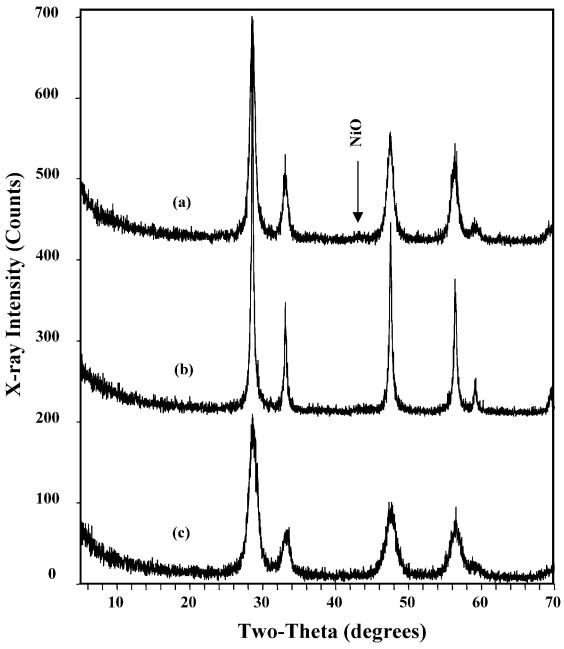

Fig. 1. XRD patterns of CeO_2 supported Ni–Rh bimetallic catalysts: (a) Ni(5)Rh(1)/CeO_2-I, (b) Ni(5)Rh(1)/CeO_2-II, (c) Ni(5)Rh(1)/CeO_2-III.

Table 2
Hydrogen chemisorption results of CeO_2 supported Ni–Rh bimetallic catalysts

Catalyst	H_2 chemisorption on Rh			H_2 chemisorption on Ni		Total H_2 uptake[d] (μmol g^{-1})
	Uptake[a] (μmol g^{-1})	D[b] (%)	dp[c] (nm)	Uptake[a] (μmol g^{-1})	D[a] (%)	
Ni(5)Rh(1)/CeO_2-I	23	47	2.3	21	4.9	44
Ni(5)Rh(1)/CeO_2-II	8	17	6.6	26	6.1	34
Ni(5)Rh(1)/CeO_2-III	40	83	1.3	9	2.0	49
Ni(5)Rh(0)/CeO_2-III	–	–	–	37	8.6	37
Ni(0)Rh(1)/CeO_2-III	17	35	3.2	–	–	17
Ni(5)/CeO_2[e]	–	–	–	34.8	8.2	34.8

[a] H_2 uptake per g of catalyst.
[b] D = metal dispersion.
[c] dp = particle diameter or crystallite size.
[d] Sum of H_2 uptake for Rh and Ni metals.
[e] Reference [21].

take for Rh metal and its dispersion are the highest for Ni(5)Rh(1)/CeO_2-III (40 μmol g^{-1} and 83%, respectively) and lowest for Ni(5)Rh(1)/CeO_2-II (8 μmol g^{-1} and 17%, respectively). Rh particle size increases in the following order: Ni(5)Rh(1)/CeO_2-III < Ni(5)Rh(1)/CeO_2-I < Ni(5)Rh(1)/CeO_2-II. The Rh metal dispersion and crystallite sizes are in accordance with the CeO_2 crystallite sizes given in Table 1. Ni(5)Rh(1)/CeO_2-III, with the smallest CeO_2 crystallite size (about 6.5 nm) exhibited the highest Rh metal dispersion (83%) and the smallest Rh particle size (about 1.3 nm). On the other hand, the large crystallite size (29.3 nm) of Ni(5)Rh(1)/CeO_2-II led to a lower Rh metal dispersion and larger particle size. It is also interesting to note that the Rh metal dispersion increased from about 35% for Ni(0)Rh(1)/CeO_2-III to about 83% for Ni(5)Rh(1)/CeO_2-III. For the same sample, the total H_2 uptake increased from 17 to 49 μmol g^{-1}.

Note that the H_2 uptake and dispersion obtained in the present study (Table 2) for Rh-free Ni/CeO_2 containing 5 wt% Ni (Ni(5)Rh(0)/CeO_2-III) is comparable with the data reported recently for 5% Ni/CeO_2 catalyst [21], supporting the validity of the method used in the present study for CeO_2-supported Ni–Rh bimetallic catalysts. It is also interesting to note that, unlike that observed for Rh, the H_2 uptake and dispersion data for Ni show the reverse trend. As can be seen, a high Ni dispersion (8.6%) was obtained in the absence of Rh, and the dispersion decreased to about 2% in the presence of 1% Rh. These results suggest that the presence of Ni in the catalyst formulations improved Rh dispersion. In contrast, the presence of Rh increased the Ni crystallite size, leading to a lower Ni metal dispersion.

3.1.2. Redox properties

The redox properties of catalysts were investigated by TPR experiments; the profiles are shown in Fig. 2. For comparison, the TPR profiles of Ni-free Ni(0)Rh(1)/CeO_2-III and of Rh-free Ni(5)Rh(0)/CeO_2-III together with Ni(10)Rh(0)/CeO_2-III containing 5 and 10 wt% Ni are also shown. The Ni-free Ni(0)Rh(1)/CeO_2-III exhibits a sharp reduction profile centered at 111 °C, attributed to the reduction of Rh^{3+} in Rh_2O_3 supported on CeO_2. The Rh-free Ni(5)Rh(0)/CeO_2-III shows broad H_2 consumption with humps at around 200, 250, and 300 °C,

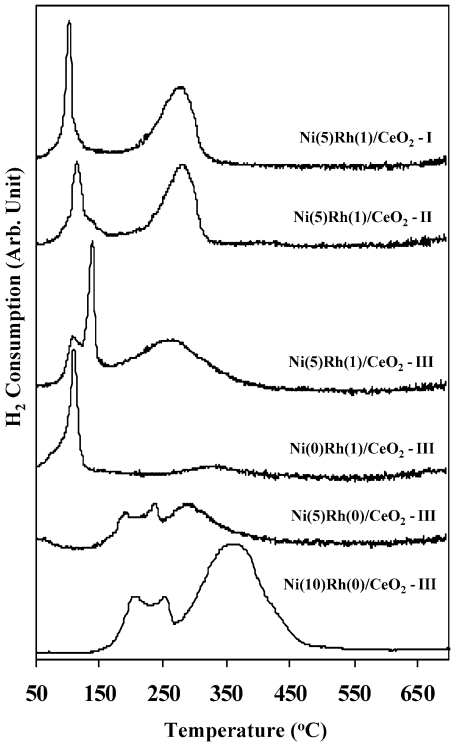

Fig. 2. Temperature-programmed reduction profiles CeO_2 supported Ni–Rh bimetallic catalysts.

attributed to the reduction of well-dispersed NiO on CeO_2 matrix. The wide H_2 consumption peak suggests a broad particle size distribution. Ni(10)Rh(0)/CeO_2-III containing 10 wt% Ni also exhibits a similarly wide H_2 consumption peak at higher temperature with increased intensity for NiO reduction.

The catalysts containing both Rh and Ni exhibit two main reduction peaks, one below 150 °C and the other at around 300 °C, for the reduction of Rh_2O_3 and NiO, respectively. It is interesting to note that the shape and the peak maximum depend on the crystallite size of the CeO_2 support. Ni(5)Rh(1)/CeO_2-I and Ni(5)Rh(1)/CeO_2-II exhibit sharp reduction peaks at 103 and 117 °C, respectively, close to the reduction peak observed in the Ni(0)Rh(1)/CeO_2-III sample containing only rhodium without nickel. In contrast, Ni(5)Rh(1)/CeO_2-III exhibits a reduction peak at higher temperature (around 150 °C), together with a shoulder at 113 °C, indicating the existence of at least two kinds of Rh^{3+} species. Mizuno et al. [22] observed a similar profile in their TPR experiments on Rh/CeO_2 catalyst and ascribed them to the reduction of Rh_2O_3 at a Rh_2O_3–CeO_2 interface and bulk-like Rh_2O_3.

A significant difference can also be seen in the reduction of the Ni^{2+} region. Both CeO_2-I- and CeO_2-II-supported catalysts show a sharp H_2 consumption peak centered at around 290 °C, whereas the CeO_2-III-supported catalyst exhibits a broad reduction peak centered at 260 °C. Whereas H_2 consumption for NiO reduction is completed at around 330 °C in both CeO_2-I- and CeO_2-II-supported catalysts, H_2 consumption continues up to around 360 °C in the CeO_2-III-supported catalyst. The higher reduction temperature of Rh_2O_3 and the wider reduction profile of NiO phases in the CeO_2-III-supported catalyst

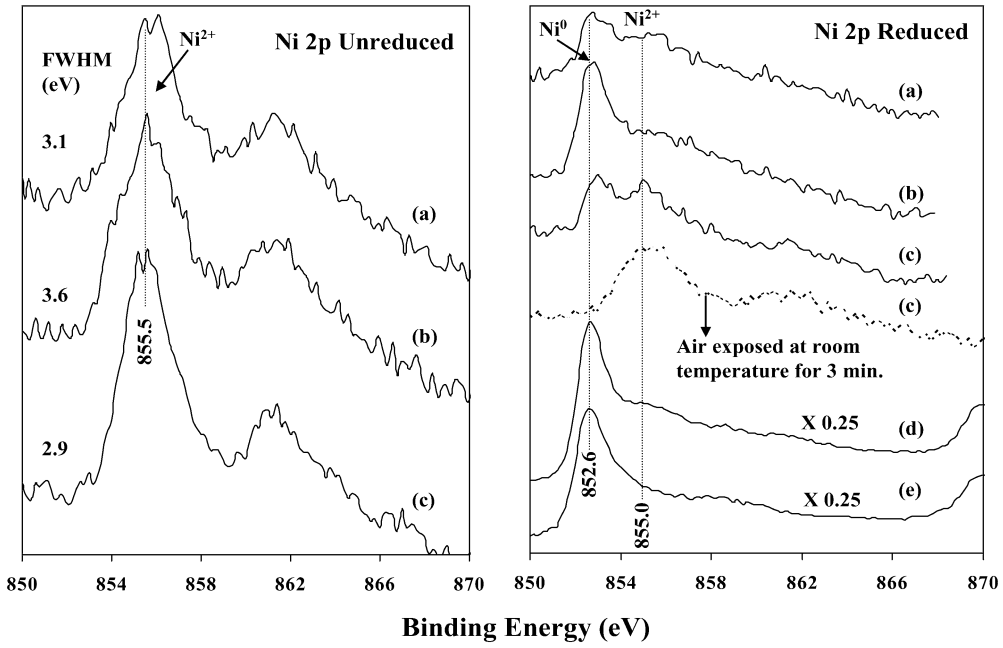

Fig. 3. Ni 2p XP spectra of CeO_2 supported Ni–Rh bimetallic catalysts: (a) Ni(5)Rh(1)/CeO_2-I, (b) Ni(5)Rh(1)/CeO_2-II, (c) Ni(5)Rh(1)/CeO_2-III, (d) Ni(10)Rh(1)/CeO_2-III, (e) Ni(10)Rh(0)/CeO_2-III. The Ni(5)Rh(1)/CeO_2-III catalyst reduced and air exposed before XPS measurement is shown in broken line.

compared to the CeO_2-I- and CeO_2-II-supported catalysts suggest the existence of a strong metal–support interaction in the CeO_2-III-supported catalyst. Furthermore, the higher Rh_2O_3 reduction temperature and lower NiO reduction temperature in Ni(5)Rh(1)/CeO_2-III compared with Ni(0)Rh(1)/CeO_2-III containing only Rh and Ni(5)Rh(0)/CeO_2-III containing only Ni suggest the existence of a synergistic interaction between the Rh_2O_3 and NiO phases in these catalysts. These results imply that the presence of Rh improves the reducibility of NiO, whereas NiO retards the reducibility of Rh_2O_3 in these catalysts.

3.1.3. Surface properties

In situ XPS studies were performed on the unreduced and reduced Ni–Rh/CeO_2 catalysts in order to determine the nature and surface exposure of nickel and rhodium species. Fig. 3 shows the Ni 2p XP spectra of both unreduced (left) and reduced (right) Ni–Rh bimetallic catalysts containing 5 wt% Ni and 1 wt% Rh on various CeO_2 supports. The unreduced (Fig. 3, left) samples show peaks around 855.5 eV together with a satellite peak around 861 eV, corresponding to the binding energy (BE) values of NiO species [23]. Although the peak maximum occurs within ±0.3 eV, the full width at half maximum (FWHM) decreases in the following order: Ni(5)Rh(1)/CeO_2-II, 3.6 eV > Ni(5)Rh(1)/CeO_2-I, 3.1 eV > Ni(5)Rh(1)/CeO_2-III, 2.9 eV, demonstrating that the homogeneity of NiO dispersion on the CeO_2 support is improved in the same order. Note from Table 1 that the crystallite sizes of the CeO_2 support also decrease in the same order. Thus, the NiO species in Ni(5)Rh(1)/CeO_2-III catalyst with smaller CeO_2 crystallite size (about 6.5 nm) is relatively more homogeneously distributed compared with that in Ni(5)Rh(1)/CeO_2-II with the largest CeO_2 crystallite size (29.3 nm).

The Ni 2p XP spectra of reduced samples (Fig. 3, right) show a peak at around 853 eV, corresponding to metallic Ni [23]. However, an additional peak at around 855.0 eV is also seen in Ni(5)Rh(1)/CeO_2-I and Ni(5)Rh(1)/CeO_2-III, indicating the existence of fraction of nickel in Ni^{2+} state in these samples. The signal intensity around 855 eV is even higher for Ni(5)Rh(1)/CeO_2-III compared with Ni(5)Rh(1)/CeO_2-I. This implies that the CeO_2-III-supported sample contains relatively more Ni^{2+} ions. Note that the TPR study (Fig. 2) showed that the NiO species in all samples could be reduced below 400 °C. Because the samples in the pseudo-in situ XPS measurements were reduced at 433 °C, there are at least three possibilities for the formation of observed Ni^{2+} species in these reduced samples: (i) reoxidation of reduced Ni metals during sample preparation for pseudo-in situ XPS measurement, (ii) strong metal–support interaction possibly leading to the formation of cationic Ni species, and (iii) a small fraction of NiO species not yet be reduced. To evaluate these possibilities, a portion of the reduced sample was exposed to air at room temperature for about 3 min, and the sample was mounted for XPS analysis in the same way as for unreduced samples.

Interestingly, Fig. 3 shows that air exposure at room temperature transforms almost all reduced Ni species into a Ni^{2+} state. Note, however, that the existence of Ni^{2+} species in Ni(10)Rh(0)/CeO_2-III containing only Ni without Rh is less significant, and the sample shows the presence of Ni mainly in the metallic state (compare traces c and e in Fig. 3, right). It is also noteworthy that almost all nickel species were present in a reduced state in NiY zeolites containing 15–30 wt% Ni studied by in situ XPS measurements in the same fashion, using the same equipment during the same period [24], thus supporting the lower likelihood of reoxidation during sample preparation.

Table 3
Surface concentrations of unreduced and reduced CeO_2 supported Ni–Rh bimetallic catalysts

Catalyst	Surface composition[a] (atom %)				
	Ni	Rh	Ce	O	C
Unreduced samples					
Ni(5)Rh(1)/CeO_2-I	3.5 (3.9)	0.48 (0.95)	27.9	58.7	9.5
Ni(5)Rh(1)/CeO_2-II	4.4 (4.9)	0.48 (0.94)	27.7	58.8	8.7
Ni(5)Rh(1)/CeO_2-III	4.2 (4.7)	0.35 (0.68)	28.1	60.2	7.2
Ni(10)Rh(1)/CeO_2-III	28.3 (39.1)	0.38 (0.92)	11.6	50.0	9.8
Ni(10)Rh(0)/CeO_2-III	28.9 (39.4)	0.00 (0.00)	12.1	52.7	6.3
Ni(0)Rh(1)/CeO_2-III	0.0 (0.0)	0.23 (0.45)	29.7	59.0	11.1
Reduced samples					
Ni(5)Rh(1)/CeO_2-I	2.6 (2.7)	0.45 (0.83)	31.1	58.0	7.9
Ni(5)Rh(1)/CeO_2-II	3.4 (3.4)	0.38 (0.67)	32.9	60.1	3.3
Ni(5)Rh(1)/CeO_2-III	2.3 (2.4)	0.20 (0.37)	31.7	60.3	5.5
Ni(10)Rh(1)/CeO_2-III	12.8 (13.7)	0.30 (0.56)	27.0	52.6	7.4
Ni(10)Rh(0)/CeO_2-III	15.5 (18.3)	0.00 (0.0)	22.2	52.8	9.9
Ni(0)Rh(1)/CeO_2-III	0.0 (0.0)	0.24 (0.43)	33.2	60.9	5.6

[a] Values in parentheses are Ni and Rh surface concentrations in wt%.

The existence of metal–support interactions in CeO_2-supported catalysts is well known [25–28]. Because CeO_2 is a redox support, the reduced Ni metals could have a strong interaction with CeO_2 at the surface such that the Ni–CeO_2 redox synergism keeps at least a part of the reduced Ni in Ni^{2+} state. The degree of Ni^0 reoxidation would depend on the extent of the metal–support interaction. A stronger metal–support interaction could effectively reoxidize the Ni^0 to Ni^{2+} at the surface. The formation of cationic $Pd^{\delta+}$ species in reduced Pd/CeO_2 catalysts due to strong metal–support interaction (SMSI) is a well-known phenomenon [26]. The observation that the Ni-rich Ni(10)Rh(0)/CeO_2-III without Rh does not exhibit the presence of Ni^{2+} species, whereas Ni(10)Rh(1)/CeO_2-III containing 1 wt% Rh together with Ni develops a shoulder around 855 eV for the presence of Ni^{2+} species, suggests that the Ni–Rh synergestic interaction favors the partial oxidation of metallic Ni to Ni^{2+}.

It is likely that the higher BET surface area and smaller CeO_2 crystallite size of the Ni(5)Rh(1)/CeO_2-III catalyst favors the strong metal–support interaction in the present catalyst system. The lower intensity of the shoulder for Ni^{2+} in Ni(10)Rh(1)/CeO_2-III containing about 10 wt% Ni compared with that of Ni(5)Rh(1)/CeO_2-III containing only about 5 wt% Ni indicates that the Ni–Rh interaction and/or Rh-promoted Ni–CeO_2 metal–support interactions are stronger when the surface Ni concentration is low and the Ni metal is highly dispersed. As shown in Table 3, the Ni surface concentrations in the reduced samples are less than that in the bulk for catalysts containing 5 wt% Ni but higher than that in the bulk for catalysts containing 10 wt% Ni.

The Rh 3d XP spectra of unreduced and reduced samples are shown in Fig. 4, and the data for various supported Rh catalysts are summarized in Table 4. The spectra of unreduced samples (Fig. 4, left) show a doublet centered at around 309 and 314 eV. These peaks correspond to the binding energy of Rh $3d_{5/2}$ and Rh $3d_{3/2}$, respectively, with a spin–orbit coupling of about 5 eV and are close to the Rh^{3+} in Rh/CeO_2 catalysts (Fig. 4).

The reduced samples (Fig. 4, right) show a doublet centered at around 307.4 and 312.2 eV similar to that observed in Rh metal and reduced Rh/CeO_2 catalyst [27,28]. The asymmetric nature of the peaks and the appearance of a shoulder at around 308 eV indicate the existence of Rh^+ species together with metallic Rh in these samples. In fact, the reduced sample exposed to air at room temperature shows an intense peak at around 308.1 eV together with a shoulder at around 307.4 eV (Fig. 4, right, trace c broken line), suggesting that the reduced Rh undergoes reoxidation to form Rh^+ species. There is no evidence for the formation of Rh^{3+} in the air-exposed

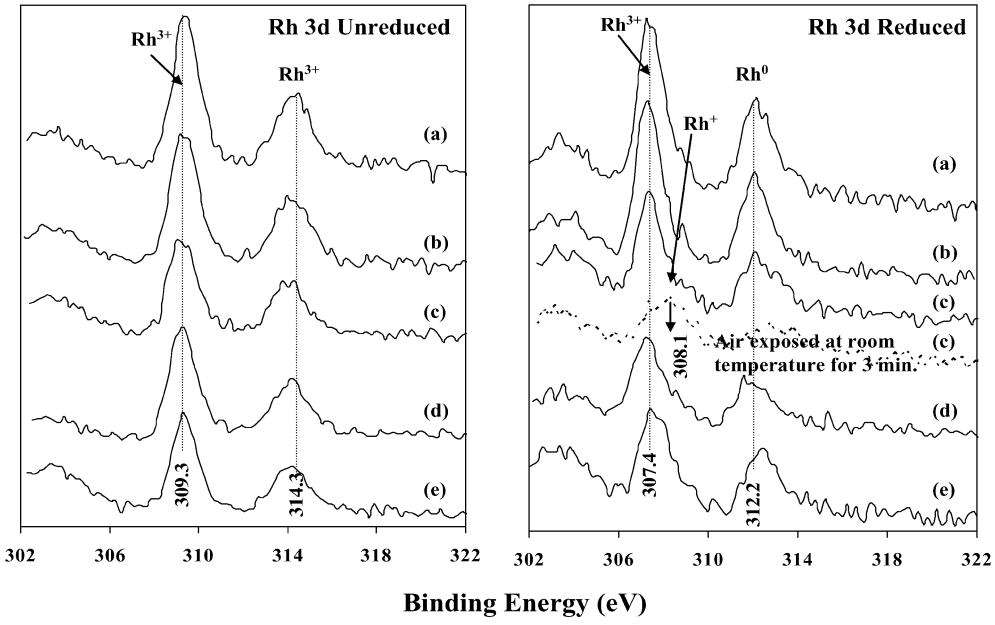

Fig. 4. Rh 3d XP spectra of CeO_2 supported Ni–Rh bimetallic catalysts: (a) Ni(5)Rh(1)/CeO_2-I, (b) Ni(5)Rh(1)/CeO_2-II, (c) Ni(5)Rh(1)/CeO_2-III, (d) Ni(10)Rh(1)/CeO_2-III, (e) Ni(0)Rh(1)/CeO_2-III.

Table 4
Rh 3d XPS data of various Rh supported catalysts

Sample	BE of $Rh_{5/2}$ (eV)	FWHM	BE of $Rh_{3/2}$ (eV)	ΔE (eV)	Reference
Unreduced					
Rh_2O_3	308.8	–	313.6	4.8	[27]
$Rh(1)/CeO_2$	308.8	–	313.6	4.8	[27]
$Ni(0)Rh(1)/CeO_2$	309.3	1.3	314.3	5.0	Present study
$Ni(5)Rh(1)/CeO_2$	309.0	1.5	314.3	5.3	Present study
$Ni(0)Rh(0.2)/ZrO_2$	308.2	2.4	NA	–	
$Ni(2)Rh(0.2)/ZrO_2$	308.9	2.8	NA	–	
$Ni(0)Rh(0.2)/La_2O_3$	307.9	2.3	NA	–	
$Ni(2)Rh(0.2)/ZrO_2$	309.1	2.1	NA	–	
Reduced					
Rh metal	307.0	NA	312.0	5.0	[27]
Rh metal	307.0	1.6	311.8	4.8	[28]
$Rh(0.5)/CeO_2$	307.3	NA	312.2	4.9	[28]
$Ni(0)Rh(1)/CeO_2$	307.4	1.6	312.2	4.8	Present study
$Ni(5)Rh(1)/CeO_2$	307.3	1.3	312.2	4.9	Present study

ΔE = spin–orbit coupling energy. NA = data not available.

sample. Noted that Kondarides and Verykios [28] reported the coexistence of Rh^0, Rh^+, and Rh^{3+} in XPS of a prereduced Rh/CeO_2 catalyst containing 0.5 wt% Rh impregnated using $RhCl_3$ salt as a precursor. In contrast, the catalyst synthesized using $Rh(NO_3)_3$ showed the existence of Rh^0 and Rh^+ but not Rh^{3+}, and these results were attributed to hindering of the Rh^{3+} reduction due to the presence of residual Cl^- species in the catalyst.

Although no significant differences in the BE and FWHM are observed with respect to Rh metal loading, the CeO_2 crystallite size strongly influences the signal intensity and the surface Rh concentration. As shown in Table 3, $Ni(5)Rh(1)/CeO_2$-III has a lower Rh concentration at the surface than the CeO_2-II- and CeO_2-I-supported catalysts. Moreover, the surface Rh concentration is lowest in the Ni-free $Ni(0)Rh(1)/CeO_2$-III, in the unreduced and reduced samples. Whereas the surface Rh content increases due to the presence of 5 wt% Ni in the unreduced sample, the Rh surface concentration further decreases in the reduced sample (Table 3).

Fig. 5 shows the XP spectra of unreduced and reduced Ni–Rh/CeO_2 catalysts in the Ce 3d region. The unreduced samples exhibit six peaks at around 882, 889, 899, 901, 908, and 917 eV that are assigned to Ce $3d_{5/2}$ $4f^2$, Ce $3d_{5/2}$ $4f^1$, Ce $3d_{5/2}$ $4f^0$, Ce $3d_{3/2}$ $4f^2$, Ce $3d_{3/2}$ $4f^1$ and Ce $3d_{3/2}$ $4f^0$, respectively for Ce^{4+} species [17,29]. In addition to these six peaks, the reduced samples exhibit shoulders at around 885 and 903 eV due to the formation of Ce^{3+} species. Because of the complex nature of the spectra, it was not possible to estimate the Ce^{4+}/Ce^{3+} ratio in the reduced sample. Closer observation of the signal intensity and surface compositions summarized in Table 3 reveals that the presence of Rh increases the surface Ce concentrations while Ni decreases in both unreduced and reduced samples.

3.2. Catalytic performance

Fig. 6 shows the effect of CeO_2 supports on the performance of Ni–Rh bimetallic catalysts for the oxidative steam reforming. The conversion was kept below 60% by using a lower reaction temperature of 300 °C and adjusting the GHSV to compare the best-case conversion and selectivities. Both ethanol conversion and H_2 selectivity decrease in the following order: $Ni(5)Rh(1)/CeO_2$-III > $Ni(5)Rh(1)/CeO_2$-I > $Ni(5)Rh(1)/CeO_2$-II. Recall that the H_2 uptake and Rh metal dispersion also decrease in the same order (Table 2), suggesting that the catalytic activity for ethanol conversion and H_2 selectivity depend on the Rh metal dispersion. In addition, the

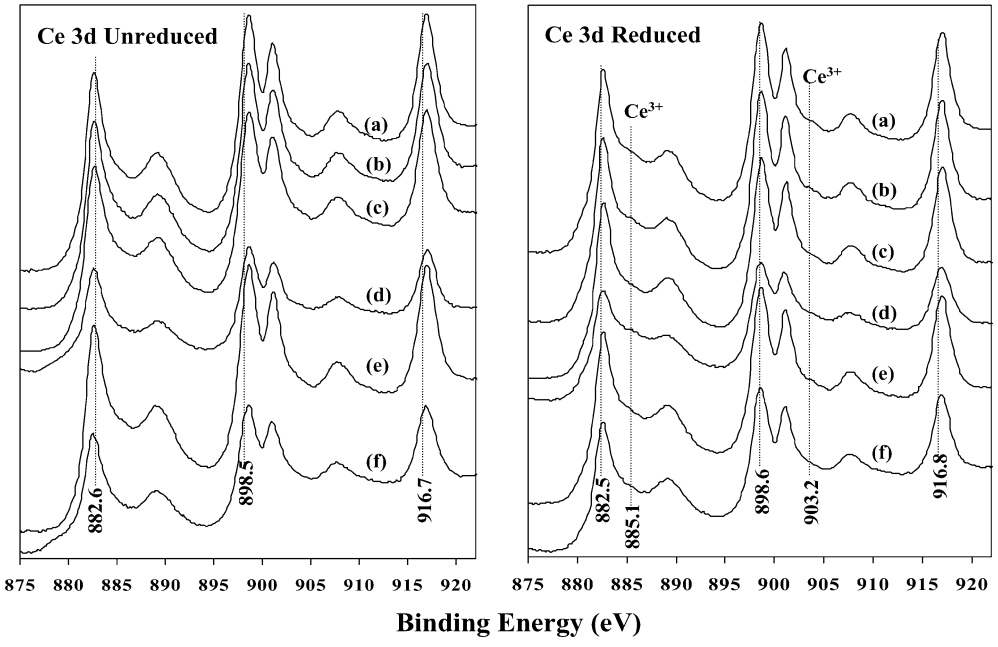

Fig. 5. Ce 3d XP spectra of CeO_2 supported Ni–Rh bimetallic catalysts: (a) $Ni(5)Rh(1)/CeO_2$-I, (b) $Ni(5)Rh(1)/CeO_2$-II, (c) $Ni(5)Rh(1)/CeO_2$-III, (d) $Ni(10)Rh(1)/CeO_2$-III, (e) $Ni(0)Rh(1)/CeO_2$-III, (f) $Ni(10)Rh(0)/CeO_2$-III.

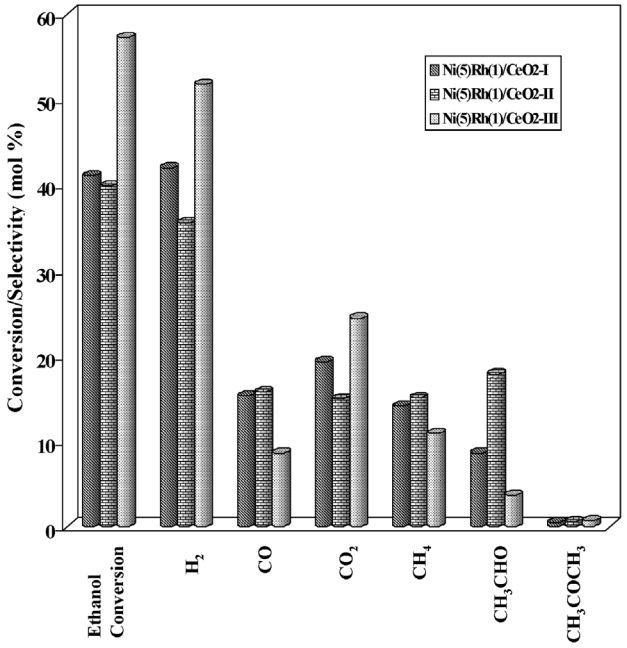

Fig. 6. Effect of CeO_2 supports on the catalytic performance in the oxidative steam reforming of ethanol over Ni–Rh/CeO_2 bimetallic catalysts; $H_2O/EtOH = 4$; $O_2/EtOH = 0.4$; GHSV = 244,000 h^{-1}.

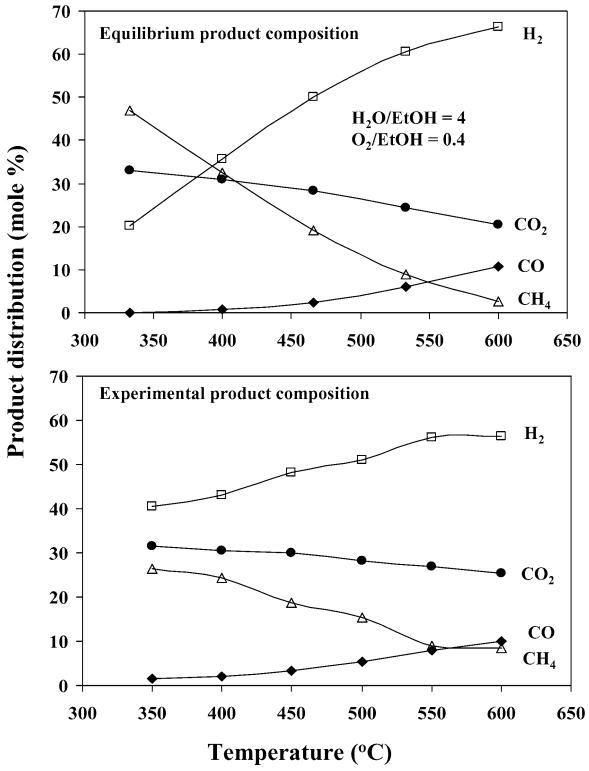

Fig. 7. Comparison of thermodynamic equilibrium compositions with actual product compositions obtained in the oxidative steam reforming of ethanol over Ni(5)Rh(1)/CeO_2-III catalyst. Data collected at the initial ethanol conversion close to 100% (below 5 h TOS) in the temperature range studied. $H_2O/EtOH = 4$; $O_2/EtOH = 0.4$; GHSV = 244,000 h^{-1}.

catalyst supported on CeO_2-III exhibits lower selectivities for undesirable byproducts, namely CO, CH_4, and CH_3CHO. This indicates that the Ni–Rh bimetallic catalyst supported on CeO_2-III is more efficient in breaking C–C and C–H bonds of ethanol to produce H_2 and CO_x. The highest conversion and lowest CH_4 selectivity (or lowest molar yield of CH_4 based on EtOH) also indicate that ethanol is more effectively reformed into H_2 and CO_x over the Ni(5)Rh(1)/CeO_2-III catalyst.

In contrast, the catalyst supported on CeO_2-II with larger CeO_2 crystallite size exhibits high selectivity for CH_3CHO and low selectivity for H_2. Note that the large CeO_2 crystallite size also decreases the Rh metal dispersion (see Table 2). Thus, the higher acetaldehyde selectivity of the Ni(5)Rh(1)/CeO_2-II catalyst is due to the lower Rh metal dispersion. The catalyst supported on CeO_2-I shows an intermediate ethanol conversion and H_2 selectivity. Based on these results, it appears that the CeO_2 crystallite size, apart from BET surface area, has a strong influence on the Rh metal dispersion, which in turn influences the catalytic activity for ethanol conversion. The smaller the CeO_2 crystallite size, the greater the Rh metal dispersion, allowing higher ethanol conversion and H_2 selectivity.

Fig. 7 compares the actual product compositions in the OSR of ethanol obtained at different temperatures (350–600 °C) with that of calculated equilibrium compositions. The ethanol conversions are close to 100% in the temperature range studied. The main products considered in the equilibrium calculations were H_2(g), H_2O(g), CO(g), CO_2(g), CH_4(g). The unconverted ethanol and other oxygenated byproducts were negligible. A comparison of experimental product compositions with thermodynamic equilibrium compositions reveals that higher H_2 and lower CH_4 distributions are obtained at lower reaction temperatures. In contrast, at higher temperatures, the experimental product compositions approach the thermodynamic equilibrium compositions. This suggests that the ethanol reforming over the present catalysts is effective and kinetically controlled at low reaction temperatures, whereas at higher temperatures, the reaction is thermodynamically controlled.

A review of recent literature on ethanol reforming indicates that the reaction is more effective at lower temperatures (300–450 °C), producing high selectivity of H_2 over base metals and/or noble metals supported on redox supports such as CeO_2, ZrO_2, and Y_2O_3 [14,30,31]. In contrast, catalysts supported on nonredox supports, such as Al_2O_3, require higher reaction temperatures (above 600 °C) [6–11,13]. It is likely that the strong metal–support interactions present in the catalysts supported on redox supports, such as CeO_2 and ZrO_2, somehow make the ethanol reforming reaction more complex, involving several elementary and consecutive reactions at low temperatures to achieve higher ethanol conversion and H_2 selectivity.

Because the Ni(5)Rh(1)/CeO_2-III catalyst exhibits the highest ethanol conversion and H_2 selectivity, its stability during on-stream operation has also been examined at three different temperatures; the results are summarized in Fig. 8. At 350 °C, ethanol conversion drops significantly after 5 h of on-stream operation. CH_4 selectivity also decreases, whereas CO selectivity increases. In contrast, stable ethanol conversion and product selectivity could be obtained at 450 and 600 °C. Relatively higher H_2 selectivity and lower CH_4 selectivity could be reached at 600 °C; however, under these operating conditions, CO selec-

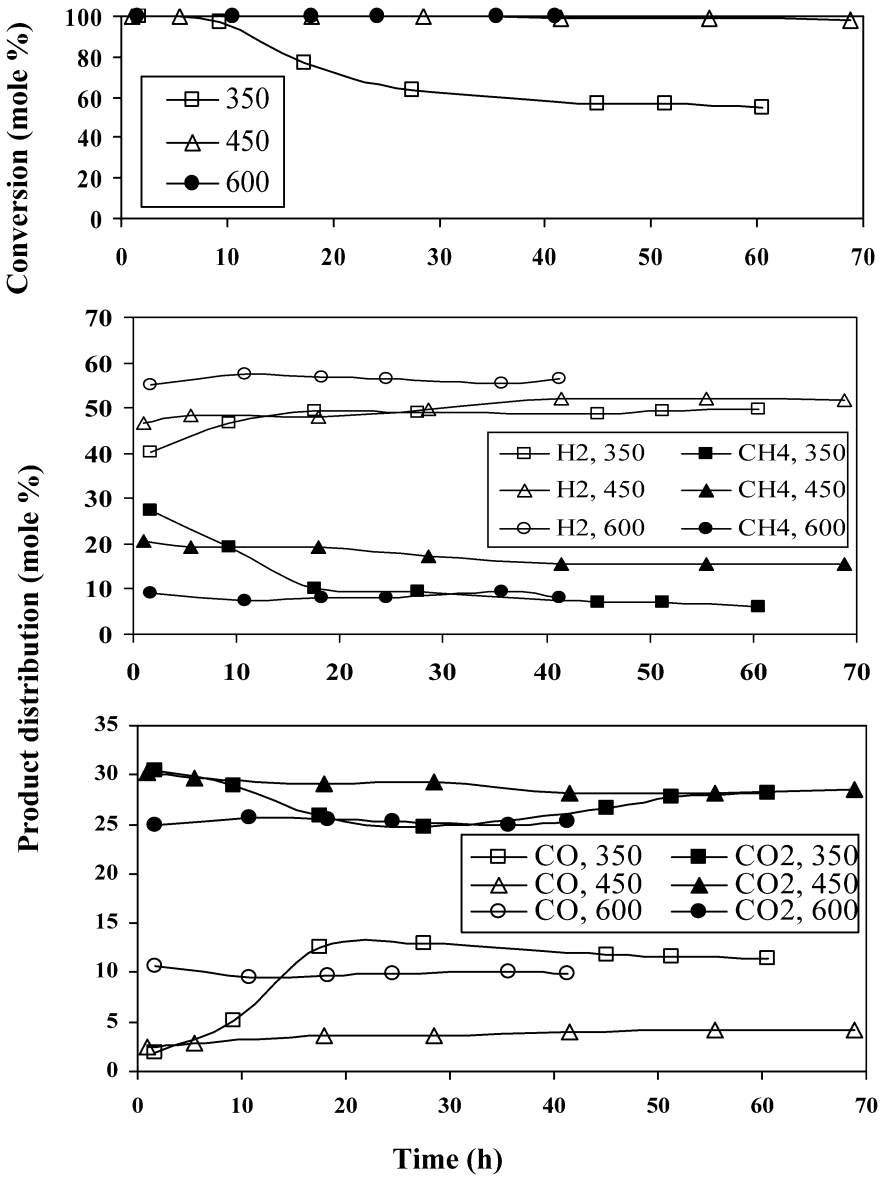

Fig. 8. Changes in catalytic activity and selectivity with time-on-stream during the oxidative steam reforming of ethanol over Ni(5)Rh(1)/CeO_2-III catalyst at different temperatures (350–600 °C); $H_2O/EtOH = 4$; $O_2/EtOH = 0.4$; GHSV = 244,000 h^{-1}.

tivity is the highest (>10%). These results suggest that CH_4 reforming is also more effective at 600 °C over the present catalyst.

The deactivation observed at 350 °C could be caused by various factors, including site blockage due to the presence of carbonaceous materials, poisoning of the catalyst surface by the reactants/products, and sintering of the active metals. Because stable activity is observed at 450 and 600 °C, it is unlikely that the sintering of active metal caused the observed deactivation. Moreover, if carbon formation were the cause, then the product distribution would be expected to remain almost unaffected. But because significant changes in the selectivities of CH_4 and CO are observed, the deactivation could be due to the passivation of the catalyst surface by the reactant and/or products. At high temperatures, these species are desorbed completely into relevant products, thereby keeping the catalyst surface clean for subsequent reactions.

4. Discussion

4.1. Effect of CeO_2 crystallite size

The dependence of catalytic activity on the textural properties, such as BET surface area and crystallite size of CeO_2, is well known for CeO_2-supported catalysts [18,19,32,33]. For instance, in their study on methane oxidation over Cu- and Ag-modified CeO_2 with different crystallite sizes and BET surface areas, Kundakovic and Flytzani-Stephanopoulos [32] found that the interaction of CeO_2 with Ag and CuO was a strong function of CeO_2 crystallite size. In the presence of transition metal or metal oxide, a smaller crystallite size of CeO_2 favored the formation of highly reducible oxygen species and enhanced methane oxidation activity. Our recent study on the oxygen-assisted water–gas shift (OWGS) reaction over Cu–Pd/CeO_2 catalysts with varying CeO_2 crystallite sizes and BET

surface areas found that higher catalytic performance was obtained over catalysts with smaller CeO_2 crystallite sizes [33]. In contrast, Wang et al. [18,19] reported that the CeO_2 crystallite size had no effect on the rate of the WGS reaction over Pd/CeO_2 catalysts with CeO_2 of particle size 7.2–40 nm.

The surface area and crystallite size of the support influence the dispersion and particle size of the supported metal, which in turn influence the catalytic activity. In fact, the structure-sensitive and structure-insensitive reactions are classified based on the influence of the metal particle size on the specific activity or turnover frequency of the given catalytic reaction [34–36].

In the present CeO_2-supported Ni–Rh bimetallic catalysts, the metal dispersions and particle sizes can be changed by varying the crystallite sizes of the CeO_2 supports. Both H_2 chemisorption and in situ XPS studies clearly demonstrate that the Rh metal dispersion increases and its particle size decreases with decreasing CeO_2 crystallite size. Higher catalytic activity for ethanol conversion and H_2 selectivity are obtained over catalysts containing highly dispersed Rh metal with a smaller particle size (around 3.2 nm). Adding Ni further improves the Rh metal dispersion and makes its particle size smaller (around 1.3 nm). These results suggest that Rh is the more active species involved in ethanol reforming and that catalytic activity increases with increasing numbers of active Rh species (i.e., Rh dispersion).

The reforming of ethanol involves breaking of a C–C bond. Cleavage of the C–C bond of an adsorbed ethoxide species requires proper orbital–orbital interaction between carbon atoms of the adsorbate and the surface [37]. This can occur only if the adsorbed species is tilted toward the surface. Spectroscopic studies on the reaction pathway of ethanol over Rh(111) single-crystal surfaces has demonstrated the formation of a cyclic five-membered oxometallate species [37,38]. The oxometallate species readily undergoes C–C bond cleavage and reforms to produce H_2 and CO_x species. A recent study on the OSR of ethanol over $Ni–Rh/CeO_2$ catalysts suggests that Rh plays a major role in breaking C–C and C–H bonds; compared with Rh, Ni is much less active for EtOH reforming, but the addition of Ni favors the water–gas shift reaction, leading to increased conversion of CO to CO_2 under the conditions used here [15].

The results of the present study suggests that the observed variations in activity and selectivity of different $NiRh/CeO_2$ catalysts can be attributed to the differences in CeO_2 supports, which can affect both the geometric (e.g., metal particle size and dispersion) and electronic (metal–support interaction) properties of catalysts.

4.2. The nature of Ni and Rh surface species

The partial transformation of Ni^0 into Ni^{2+} and of Rh^0 into Rh^+ on air exposure of the present catalyst system (Figs. 3 and 4) clearly suggests that the Ni and Rh in these catalysts are present as highly dispersed metallic species rather than a Ni–Rh surface alloy. The presence of separate reduction peaks for Ni^{2+} and Rh^{3+} at two distinctly different temperatures (TPR in Fig. 2) and a dramatic increase in the total H_2 consumption from 17 μmol g^{-1} for $Ni(0)Rh(1)/CeO_2$-III to 49 μmol g^{-1} for $Ni(5)Rh(1)/CeO_2$-III (Table 2) further suggests the absence of NiRh surface alloy in the present catalyst system. Studies on various bimetallic catalyst systems, such as Ni–Rh, Ni–Ru, and Co–Ru supported on CeO_2, ZrO_2, La_2O_3, and Al_2O_3, however, have revealed surface alloy formation [39–44]. The formation of surface alloy in those catalytic systems led to the simultaneous reduction of Ni and Ru in the Ni–Ru bimetallic catalyst and of Co and Ru in the Co–Ru bimetallic catalyst in TPR experiments [41,42]. In some cases, the formation of surface alloy also impaired H_2 or CO chemisorption. In their H_2 chemisorption studies on $Ni–Rh/La_2O_3$ catalysts, Irusta et al. [39,40] observed that the H_2/metal ratio decreased from 0.82 for $Rh(2\%)/La_2O_3$ to 0.60 for $Ni(2\%)–Rh(0.2\%)/La_2O_3$. Similarly, Jozwiak et al. [43] reported a dramatic decrease in H_2 uptake from 0.73 $cm^3\,g^{-1}$ for $Rh(5\%)/SiO_2$ to 0.43 for $Ni(2.5\%)–Rh(2.5\%)/SiO_2$. Based on these results, Ni and Rh in the present CeO_2-supported Ni–Rh bimetallic catalysts are likely present as highly dispersed redox species rather than as a surface alloy.

5. Conclusion

Our findings demonstrate that the use of different CeO_2 supports with varying surface areas and crystallite sizes can lead to major differences in the physicochemical and catalytic properties of CeO_2-supported Ni–Rh bimetallic catalysts for the oxidative steam reforming of ethanol. The crystallite size of CeO_2, apart from its surface area, has a strong influence on the metal dispersion of Ni–Rh catalysts. The catalytic activity for ethanol conversion and H_2 selectivity depends strongly on Rh particle size and dispersion. The smaller the CeO_2 crystallite size, the higher the Rh metal dispersion and consequently the higher the catalytic activity for ethanol conversion and H_2 selectivity. Ni–Rh bimetallic catalyst supported on nanocrystalline CeO_2 (crystallite size of about 6.5 nm) (CeO_2-III) exhibited stable activity and selectivity during on-stream operations of oxidative steam reforming at 450 and 600 °C.

Analytical characterization of the catalysts revealed the following trends. The reduced Ni and Rh species were reversibly oxidized, suggesting the existence of a highly dispersed Ni–Rh redox couple on CeO_2 rather than a NiRh alloy in the present catalyst system. The presence of Ni improved Rh dispersion. The Rh species were highly dispersed over nanocrystalline CeO_2 with the smallest crystallite size (about 6.5 nm). Smaller CeO_2 crystallite size led to a stronger $Rh–CeO_2$ metal–support interaction as well as a synergistic Ni–Rh interaction in the Ni–Rh bimetallic catalysts.

The present work clearly demonstrates a case in which significant differences in properties (such as metal dispersion) and performance (such as activity and selectivity) of different $NiRh/CeO_2$ catalysts can be attributed to the differences in CeO_2 supports. It also indicates that the supports can influence both the geometric (e.g., metal particle size and dispersion) and electronic (e.g., metal–support interaction) properties of the supported Ni–Rh bimetallic catalysts for oxidative steam reforming of ethanol.

Acknowledgments

The authors are grateful to the Nippon Shokubai Co., Ltd, and Pennsylvania State University for supporting this work and to Rhodia Chemicals Company for its generous gift of the CeO_2 samples. The Environmental Molecular Sciences Laboratory (EMSL), a national scientific user facility at Pacific Northwest National Laboratory (PNNL), Richland, WA is gratefully acknowledged for XPS measurements under proposal 6300. Chunshan Song thanks the U.S. Department of State and the U.S.–U.K. Fulbright Commission for the Fulbright Distinguished Scholar award in conjunction with his sabbatical stay at Imperial College London, University of London.

References

[1] C.S. Song, Catal. Today 77 (2002) 17.
[2] D.L. Trimm, Z.I. Onsan, Catal. Rev.-Sci. Eng. 43 (2001) 31.
[3] J.R. Rostrup-Nielsen, Phys. Chem. Chem. Phys. 3 (2001) 283.
[4] S. Velu, N. Satoh, C.S. Gopinath, K. Suzuki, Catal. Lett. 82 (2002) 145.
[5] G.A. Deluga, J.R. Salge, L.D. Schmidt, X.E. Verykios, Science 303 (2004) 993.
[6] S. Cavallaro, V. Chiodo, A. Vita, S. Freni, J. Power Sources 123 (2003) 10.
[7] D.K. Liguras, D.I. Kondarides, X.E. Verykios, Appl. Catal. B 43 (2003) 345.
[8] J.P. Breen, R. Burch, H.M. Coleman, Appl. Catal. B 39 (2002) 65.
[9] A.N. Fatsikostas, D.I. Kondarides, X.E. Verykios, Catal. Today 75 (2002) 145.
[10] S. Cavallaro, V. Chiodo, S. Freni, N. Mondello, F. Frusteri, Appl. Catal. A: Gen. 249 (2003) 119.
[11] V. Fierro, O. Akdim, C. Mirodatos, Green Chem. 5 (2003) 20.
[12] V. Fierro, V. Klouz, O. Akdim, C. Mirodatos, Catal. Today 75 (2002) 141.
[13] R.M. Navarro, M.C. Alvarez-Galvan, M.C. Sanchez-Sanchez, F. Rosa, J.L.G. Fierro, Appl. Catal. B: Environ. 55 (2005) 229.
[14] C. Diagne, H. Idriss, K. Pearson, M.A. Gomez-Garcia, A. Kiennemann, C.R. Chimie 7 (2004) 617.
[15] J. Kugai, S. Velu, C.S. Song, Catal. Lett. 101 (2005) 255.
[16] J. Kugai, S. Velu, C.S. Song, M.H. Engelhard, Y.-H. Chin, Prepr. Pap.-Am. Chem. Soc., Div. Pet. Chem. 49 (2004) 346.
[17] M.A. Henderson, C.L. Perkinds, M.H. Engelhard, S. Thevuthasan, C.H.F. Peden, Surf. Sci. 526 (2003) 1.
[18] X. Wang, R.J. Gorte, J.P. Wagner, J. Catal. 212 (2002) 225.
[19] X. Wang, R.J. Gorte, Appl. Catal. A: Gen. 224 (2002) 209.
[20] T. Zhu, M. Flytzani-Stephanopoulos, Appl. Catal. A: Gen. 208 (2001) 403.
[21] S. Pengpanich, V. Meeyoo, T. Rirksomboon, Catal. Today 93–95 (2004) 95.
[22] T. Mizuno, Y. Matsumura, T. Nakajima, S. Mishima, Int. J. Hydrogen Energy 28 (2003) 1393.
[23] S. Velu, K. Suzuki, M. Vijayaraj, S. Barman, C.S. Gopinath, Appl. Catal. B: Environ. 55 (2005) 287.
[24] S. Velu, C.S. Song, M.H. Engelhard, Y.-H. Chin, Ind. Eng. Chem. Res. 44 (2005) 5740.
[25] C. Force, J.P. Belzunegui, J. Sanz, A. Martinez-Arias, J. Soria, J. Catal. 197 (2001) 192.
[26] K. Sun, W. Lu, M. Wang, X. Xu, Appl. Catal. A: Gen. 268 (2004) 107.
[27] A. Gayen, K.R. Priolkar, R. Sarode, V. Jayaram, M.S. Hegde, G.N. Subbabba, S. Emura, Chem. Mater. 16 (2004) 2317.
[28] D.I. Kondarides, X.E. Verykios, J. Catal. 174 (1998) 52.
[29] J.P. Holgodo, R. Alvarez, G. Munuera, Appl. Surf. Sci. 161 (2000) 301.
[30] J. Sun, X. Qiu, F. Wu, W. Zhu, W. Wang, S. Hao, Int. J. Hydrogen Energy 29 (2004) 1075.
[31] J. Sun, X.-P. Qiu, F. Wu, W.-T. Zhu, Int. J. Hydrogen Energy 30 (2005) 437.
[32] Lj. Kundakovic, M. Flytzani-Stephanopoulos, J. Catal. 179 (1998) 203.
[33] E.S. Bickford, S. Velu, C.S. Song, Catal. Today 99 (2005) 347.
[34] P.M. Holmblad, D.R. Rainer, D.W. Goodman, J. Phys. Chem. B 101 (1997) 8883.
[35] F.J. Gracia, L. Bollmann, E.E. Wolf, J.T. Miller, A.J. Kropf, J. Catal. 220 (2003) 382.
[36] R.S. Rao, A.B. Walters, M.A. Vannice, J. Phys. Chem. B 109 (2005) 2086.
[37] P.-Y. Sheng, A. Yee, G.A. Bowmaker, H. Idriss, J. Catal. 208 (2002) 393.
[38] N.F. Brown, M.A. Barteau, J. Phys. Chem. 98 (1994) 12737.
[39] S. Irusta, L.M. Cornaglia, E.A. Lombardo, J. Catal. 210 (2002) 7.
[40] S. Irusta, L.M. Cornaglia, E.A. Lombardo, J. Catal. 210 (2002) 263.
[41] M. Cerro-Alarcon, A. Maroto-Valiente, I. Rodriguez-Ramos, A. Guerrero-Ruiz, Appl. Catal. A: Gen. 275 (2004) 257.
[42] P.C. Das, N.C. Pradhan, A.K. Dalai, N.N. Bakhshi, Fuel Process. Technol. 85 (2004) 1487.
[43] W.K. Jozwiak, M. Nowosielska, J. Rynkowski, Appl. Catal. A: Gen. 280 (2005) 233.
[44] T. Miyake, T. Asakawa, Appl. Catal. A: Gen. 280 (2005) 47.